




Measurement of mass and total kinetic energy distributions for the $^{12}\text{C} + ^{175}\text{Lu}$ system

Sangeeta Dhuri ^{1,2}, K. Mahata ^{1,2,*}, A. Shrivastava,^{1,2} K. Ramachandran,¹ S. K. Pandit,¹ Vineet Kumar,¹ V. V. Parkar,^{1,2} P. C. Rout,^{1,2} A. Kumar,¹ Arati Chavan,³ Satbir Kaur,^{1,2} and T. Santhosh ^{1,2}

¹Nuclear Physics Division, Bhabha Atomic Research Centre, Mumbai 400085, India

²Homi Bhabha National Institute, Anushaktinagar, Mumbai 400094, India

³Vivekanand Education Society's College of Arts, Science and Commerce, Mumbai 400071, India



(Received 17 May 2022; accepted 8 July 2022; published 21 July 2022)

Fission fragment mass and total kinetic energy (TKE) distributions were measured for $^{12}\text{C} + ^{175}\text{Lu}$ system at excitation energies down to 16.7 MeV above the saddle point. The overall mass and TKE distributions could be fitted with single Gaussian functions. The observed width of the mass and TKE distributions agree well with the systematics based on liquid drop (LD) behavior. The average TKE also shows parabolic dependence on fragment mass, as expected from LD behavior. Small contributions due to microscopic corrections from $Z \approx 38$ and 45 shells can be extracted, if the widths of the LD component are fixed from systematics. Contrary to the theoretical predictions of substantial contributions from microscopic corrections, dominance of liquid drop behavior was observed.

DOI: [10.1103/PhysRevC.106.014616](https://doi.org/10.1103/PhysRevC.106.014616)

I. INTRODUCTION

Nuclear fission is one of the most intricate processes of nuclear decay, where a heavy nucleus splits into two or more lighter nuclei having similar masses, releasing large amount of energy. The fission process was explained using the liquid drop model (LDM), which considers the nucleus as an incompressible macroscopic liquid drop [1,2]. However, the LDM could not explain the predominant asymmetric mass split at low excitation energy in the actinide region. The incorporation of microscopic effects such as shell corrections to the macroscopic liquid drop (LD) paved the way to understanding the observed mass asymmetry [3]. The potential energy landscape with multiple valleys created by the microscopic corrections was found to strongly influence the characteristics, e.g., mass split, total kinetic energy (TKE), and neutron multiplicities in low energy fission of actinides. The concept of different fission modes, i.e., “superlong” (SL) symmetric fission mode and asymmetric “standard” fission modes ($S1$ and $S2$) was introduced [4].

Over the years, a vast knowledge base of fission of actinides has been created and is still being enriched experimentally as well as theoretically [5–7]. However, the low energy fission of preactinide nuclei remained less explored, as the increase in liquid drop fission barrier height with decreasing fissility drastically reduces fission probability at low energies. It also was expected that the liquid drop (symmetric) fission will dominate in the preactinide region. In 1980s, series of measurements were carried out by Itkis *et al.* [8–10] by bombarding p and α particles on stable preactinide targets. Symmetric fission was indeed found to dominate in this

region. It was demonstrated that the yields of asymmetric components ($S1$ and $S2$), which are very dominant in the actinide region, diminish with decreasing N and Z of the fissioning nuclei and vanish at ^{201}Tl . Flattening or a slight dip in the mass distribution around half the mass of the fissioning nucleus (A_{CN}) was also observed in most of the cases. It was interpreted in terms of positive shell corrections at $A_{CN}/2$ in contrast to negative shell corrections for $S1$ and $S2$. Later, the flattening of the mass distributions at $A_{CN}/2$ was attributed to two strongly deformed neutron shells in the nascent fragments with neutron numbers $N_1 \approx 52$ and $N_2 \approx 68$ [11].

Recent unexpected observation of almost exclusive asymmetric fission in neutron-deficient ^{180}Hg [12] at low energy has put the focus back on this region. From the liquid drop as well as spherical shell gaps perspective, splitting into two symmetric doubly magic ^{90}Zr fragments ($N = 50$, $Z = 40$) should have been the most favored. Several other measurements [13–23] have firmly established the presence of asymmetric fission in this region. However, it is still not clear what drives the asymmetry in fission of preactinides. Theoretical models based on different approaches, e.g., Brownian shape motion on the macroscopic-microscopic potential energy surface [24], the improved scission point model [25], and the time independent microscopic model [26], have interpreted these observations differently. The macroscopic-microscopic model [27,28] attributed this to the saddle asymmetry and predicted a region of asymmetry centered around ^{186}Pt . Calculations based on the microscopic energy density functional (EDF) framework [26,29] result in shell gaps at $N = 52–56$ and $Z = 34–38$, $42–46$ due to quadrupole-octupole correlations. A recent systematic study of the experimental results has demonstrated the dominance of proton shells ($Z \approx 36$) [29] in the light fragment in deciding the asymmetric split in the preactinide region, in contrast to

*Corresponding author: kmahata@barc.gov.in

the actinide region, where the heavy fragment charge ($Z \approx 52\text{--}56$) determines the mass split. The role of deformed shell gaps at $Z \approx 36\text{--}38$ and $45\text{--}46$ has been also observed in other experimental studies [19,22,23].

In the present study, measurements of fragment mass and TKE distributions for $^{12}\text{C} + ^{175}\text{Lu} \rightarrow ^{187}\text{Ir}$ were carried out. ^{187}Ir is situated around the center of the island of asymmetry predicted by the macroscopic-microscopic model [27]. It also has $2 \times (Z \approx 38, N \approx 56)$ configuration. As discussed above, the $Z \approx 38$ and $N \approx 56$ shells are identified to drive the asymmetry in the preactinide region. In case of heavy fermium isotopes, the fission characteristics change drastically while approaching ^{264}Fm ($2 \times ^{132}\text{Sn}$). Thus it would be interesting to study the fission properties of the present system. More measurements are also required to distinguish different contributions to the mass distribution and to understand their evolution across the preactinide region.

The paper is organized as follows. The experimental details are given in Sec. II. In Sec. III, the results are discussed: the experimental mass-TKE correlations, mass distributions, and mass widths are discussed in Secs. III A, III B, and III C, respectively. The various theoretical predictions are discussed in Sec. III D followed by a summary and conclusion in Sec. IV

II. EXPERIMENTAL DETAILS

The experiment was performed at the BARC-TIFR Pelletron-LINAC facility, Mumbai. A $250 \mu\text{g}/\text{cm}^2$ thick ^{175}Lu target on $170 \mu\text{g}/\text{cm}^2$ thick Al backing was mounted inside a 1.5 m wide scattering chamber. The target was mounted such that the incoming beam was first faced by the target. The bunched beam of ^{12}C was bombarded on the target at energies 58, 65, 70, and 75 MeV. The time interval between the bunches was 106.7 ns. The time structure of the bunch was monitored continuously by detecting γ rays in a BaF₂ detector placed at the beam dump. The typical width (σ) of the bunch was ≈ 0.6 ns. Two position-sensitive multiwire proportional chambers (MWPCs) [30] of active area $125 \text{ mm} \times 75 \text{ mm}$ were used for detection of fission fragments in coincidence. MWPCs were kept at angles 113° and -50° at a distance of 24 cm from the target. The time of flight (TOF) with respect to the arrival of the beam pulse, position (x, y), and the energy loss information of both the fragments in the detectors were recorded event by event. The radio-frequency (RF) signal from the beam buncher filtered by the OR of the MWPC cathode signals was used as the arrival time of the beam pulse. The target was kept at 40° with respect to the normal to the beam axis to minimize the energy loss of the fragment in the target. Two silicon surface barrier (SSB) detectors were kept at angles $\pm 20^\circ$ to monitor the current.

III. RESULTS AND DISCUSSION

As shown in Fig. 1(a), the fission events could be separated well from the quasi-elastic events using the correlation in the TOFs (T_1 vs T_2). The velocity vectors of the fragments were extracted using the position and TOF information. The measured folding angle ($\theta_1 + \theta_2$) and the total azimuth angle ($\phi_1 + \phi_2$) distributions are Gaussian in shape with peak

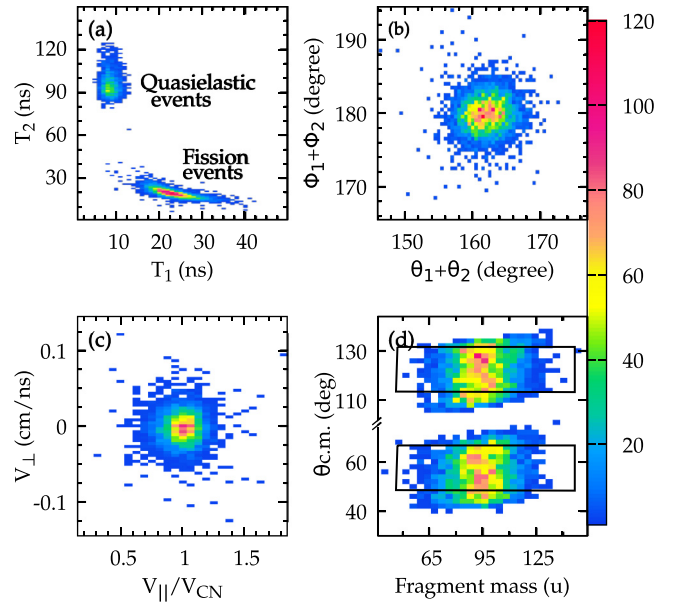


FIG. 1. Correlation plots for the (a) times of flight (T_1 and T_2), (b) folding angle ($\theta_1 + \theta_2$) and total azimuthal angle ($\phi_1 + \phi_2$), (c) parallel and perpendicular components of velocity (V_{\parallel} and V_{\perp}), and (d) mass-angle distribution (MAD) for the $^{12}\text{C} + ^{175}\text{Lu}$ system at $E_{\text{Lab}} = 65$ MeV. The V_{\parallel} is normalized by the velocity of the center of mass (V_{CN}). Plots (b)–(d) are generated for fission events.

around the expected folding angle according to Viola systematics [31] and 180° for all the incident energies, respectively. The azimuthal and folding angle distribution and the correlation plots between parallel and perpendicular components of velocity $V_{\parallel}/V_{\text{CN}}$ and V_{\perp} [Figs. 1(b) and 1(c)] confirm the two-body nature or the absence of incomplete momentum transfer (IMT) events in the reaction. It should be noted here that a significant presence of IMT events or incomplete fusion (ICF) was observed in the measurement of cross section and recoil range distribution of the evaporation residues [32,33] in the same energy range for the present system. It was interpreted that the IMT/ICF events mainly originate when ^8Be is captured by the target, forming $^{183}\text{Re}^*$, and α moves as a spectator. The ICF product, $^{183}\text{Re}^*$, has lower fissility and excitation energy as compared to the compound nucleus. Thus IMT/ICF is not expected to contribute significantly in the fission channel. The preneutron mass of the fragment (M) was calculated using the TOF difference method [34]. Small corrections due to energy loss of the fragments in the target and the backing foils (only for the forward moving fragments) are obtained event-by-event in an iterative manner taking the range-energy information from SRIM [35]. The nuclear charge of the fragment was obtained under the unchanged charge distribution (UCD) [36]. The typical correction in width of the mass distribution due to energy loss correction is observed to be about 5%. The mass resolution (σ) of the setup was estimated to be 3 u from the elastic peak. Typical mass-angle distribution (MAD) is shown in Fig. 1(d). The MAD correlation spectra do not show the presence of fast quasifission, as explained in Ref. [37]. The rectangular cut shown in the MAD plot is used to select the detector area, which is not biased

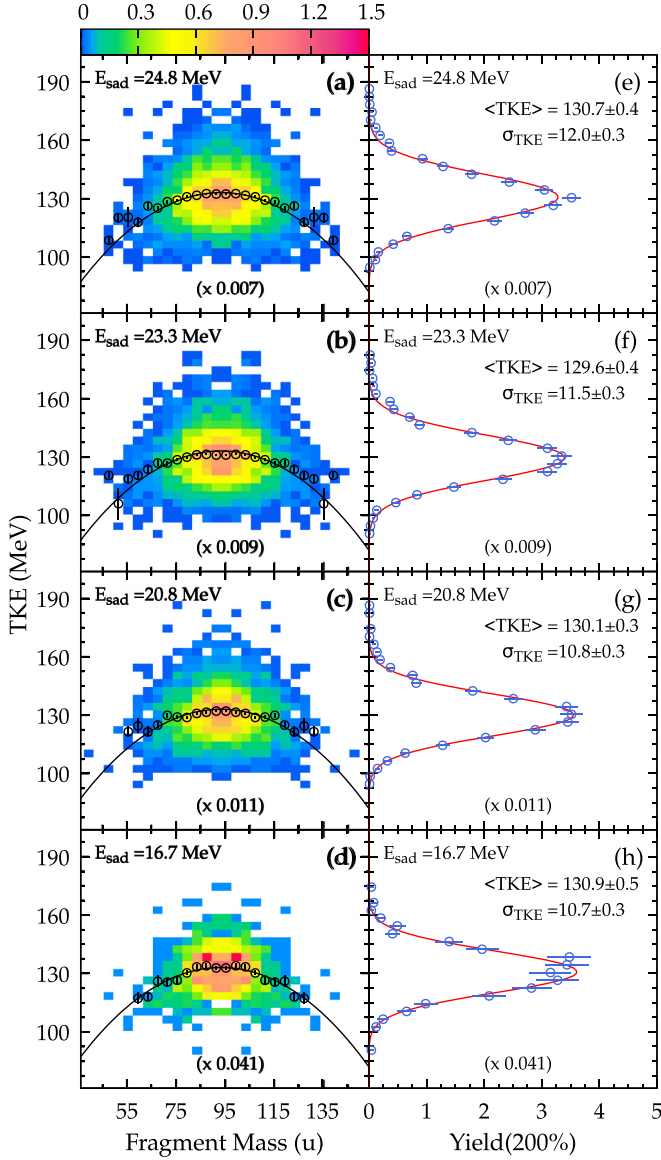


FIG. 2. Left panels (a)–(d): The fragment mass-TKE correlations along with TKE profile (black open circle). The black solid line is the LD-predicted mass dependence of TKE [38]. Right panels (e)–(h): The experimental TKE distributions are compared with the single Gaussian fits (solid line). To use the same color gradient, the distributions are normalized to 200% and the normalization factors are mentioned in the brackets.

towards a specific mass region. The rest of the analysis is done for events that are within this gate. The error bars shown in the measured mass and TKE distributions are statistical in nature.

A. Mass-TKE correlation

The mass-TKE correlations along with the TKE profile (average as a function of fragment mass) are shown in Figs. 2(a)–2(d). The liquid drop model of fission predicts a parabolic dependence of TKE on fragment mass (M) follow-

ing an equation of the form [38]

$$\text{TKE}(M) \propto \frac{M(A_{CN} - M)}{M^{1/3} + (A_{CN} - M)^{1/3}}. \quad (1)$$

Any deviation from the parabolic dependence indicates the presence of a microscopic correction. The above equation describes the measured mass dependence of TKE [Figs. 2(a)–2(d)] very well at all the energies. The TKE distributions [Figs. 2(e)–2(h)] are found to be Gaussian in shape. The mean TKE values are in good agreement with the prediction of Viola systematics (≈ 131 MeV) [31]. The widths of the measured TKE distributions are in the range from 10.7 to 12.0 MeV, which is in agreement with the observed systematic behavior [23,39] for this region. A deviation from Gaussian shape or from the systematics of width is expected if microscopic corrections are present.

B. Mass distribution

The extracted preneutron mass distributions at different excitation energies above the saddle (E_{sad}) are shown in Figs. 3(a)–3(d). The available experimental mass distribution data for the $p + {}^{186}\text{Os}$ [10] system populating the same compound nucleus are also shown in Figs. 3(e) and 3(f). It can be seen that the measured mass distributions are dominantly symmetric and can be described well by single Gaussian fits. However, at lower excitation energies slight deviation from single Gaussian can be observed around the center of the mass distribution. As discussed earlier, $Z \approx 38$ and 45 shells are expected to influence the mass distribution in this mass region. For the present case (${}^{187}\text{Ir}$), $Z \approx 38$ would correspond to symmetric fission in addition to LD symmetric fission. However, the $Z \approx 38$ component is expected to be narrower than the LD component, as the microscopic corrections varies more faster than the LD potential. The contributions of different shells are weak compared to the LD contribution, hence it is not possible to extract each of these components from an independent free fit. However, the microscopic contributions ($Z \approx 38$ and 45) can be extracted, if the width of the LD component is fixed from its systematic behavior [39]. Further, the widths of the microscopic components are varied 3–7 u depending on the excitation energy. The Z of fragments are estimated from the measured mass under UCD assumption. A similar approach has also been adopted in recent studies [22,23,29]. For the asymmetric fission, the light fragment (A_L) and the complementary heavy fragment (A_H) peaks are considered to have the same width and area. Further, the mean positions of the light (\bar{A}_L) and heavy fragment (\bar{A}_H) distributions are constrained as $\bar{A}_L + \bar{A}_H = A_{CN}$. As only the mass ratio can be determined from the method adopted in the present measurement, the counts in the lower and upper halves are strictly correlated. Thus only the lower halves of the distributions are considered while fitting. As shown in Fig. 3, such fits result in about 88% LD component at the lowest energy, which gradually increases to 100% with the increase in excitation energy.

C. Mass widths

Since the mass distributions are dominated by the LD contribution, we have analyzed the widths in terms of the

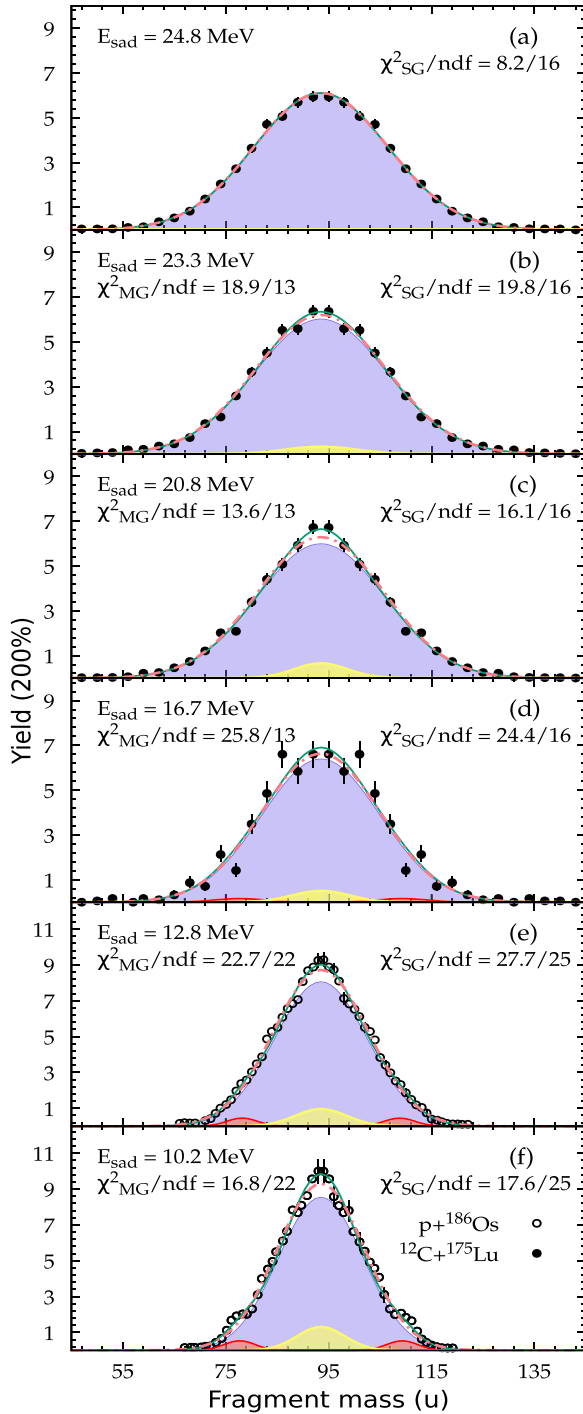


FIG. 3. The experimental mass distributions (a)–(d) for the $^{12}\text{C} + ^{175}\text{Lu}$ reaction from the present measurement (filled circles) and (e)–(f) for the $p + ^{186}\text{Os}$ reaction [10] (open circles) are plotted with increasing excitation energy at the saddle point (E_{sad}) from bottom to top panels. The solid lines show the multi-Gaussian (MG) fits to the data along with different fissioning modes corresponding to macroscopic liquid drop component (violet shaded region) and microscopic component due to $Z \approx 38$ (yellow shaded region) and $Z \approx 45$ (red shaded region) shells. The dot-dashed line is the single Gaussian (SG) fit to the data. The corresponding χ^2 and the number of degrees of freedom (ndf) are also mentioned.

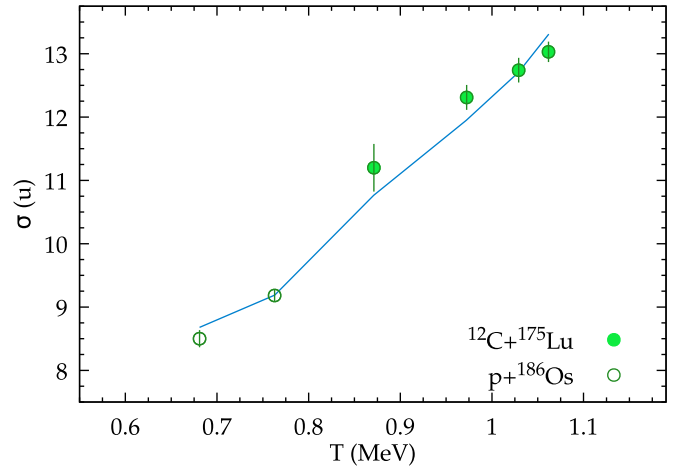


FIG. 4. The extracted mass widths from single Gaussian fits (σ_M) are plotted as a function of temperature at the saddle point (T) for present measurement $^{12}\text{C} + ^{175}\text{Lu}$ (filled circles) and $p + ^{186}\text{Os}$ [10] (open circles). The solid line is the description using Eq. (2).

statistical relation [39]

$$\sigma_{MR}^2 = \lambda T + \kappa \langle \ell_{\text{fis}}^2 \rangle. \quad (2)$$

The temperature at the saddle (T) and the ℓ^2 average of the fissioning nuclei ($\langle \ell_{\text{fis}}^2 \rangle$) are tabulated in Table I along with other relevant quantities. The fusion ℓ distributions, calculated using the CCFULL code [40] after fitting the fusion excitation function for the $^{12}\text{C} + ^{175}\text{Lu}$ system [32], were used as an input for the statistical model calculations using the code PACE [41,42] to estimate the values of average angular momentum ($\langle \ell_{\text{fis}} \rangle$), average square angular momentum ($\langle \ell_{\text{fis}}^2 \rangle$), prefission neutron multiplicity (ν_{pre}), and average energy removed by precession neutron emission (E_{eva}). The temperature at the saddle point was calculated as $T = \sqrt{E_{\text{sad}}/a}$ with $a = A/8.5$. The effective excitation energy of the fissioning nucleus at saddle is calculated as $E_{\text{sad}} = E_{\text{CN}}^* - B_{f,(\ell_{\text{fis}})} - \Delta E_{\text{eva}} - E_{\text{rot}}$. The average ℓ -dependent fission barrier heights $B_{f,(\ell_{\text{fis}})}$ are calculated using $B_{f,(\ell_{\text{fis}})} = B_{f,0} - \Delta B_{f,(\ell_{\text{fis}})}$, with $B_{f,0}$ the value of fission barrier height at zero angular momentum taken from Ref. [43]. The change in the fission barrier due to rotation (ΔB_f) and the rotational energy at the equilibrium deformation (E_{rot}) are taken from the rotating finite range model (RFRM) [44]. Though the entrance channel mass asymmetry parameters for $p + ^{186}\text{Os}$ (0.98) and the present system (0.87) are very different, they are much larger than the Businaro-Gallone critical mass asymmetry parameter ($\alpha_{BG} = 0.81$). Thus both systems are expected to exhibit characteristics of statistical decay of a fully equilibrated compound nucleus. As shown in Fig. 4, experimental mass widths for $p + ^{186}\text{Os}$ and the present system could be simultaneously fitted well using the statistical relation given in Eq. (2), indicating the absence of any significant entrance channel dependence. The resulting parameters are $\lambda = (3.12 \pm 0.12) \times 10^{-3}$ and $\kappa = (1.93 \pm 0.24) \times 10^{-6}$. These values are similar to the values obtained for nearby systems $^{16}\text{O} + ^{175}\text{Lu}$ [18] and $^{16}\text{O} + ^{186}\text{W}$ [45]. The extracted value of the stiffness

TABLE I. The laboratory energies E_{Lab} and respective compound nuclear excitation energies E_{CN}^* are listed in columns 1 and 2; columns 3 to 8 are the calculated values of average angular momenta $\langle l \rangle_{\text{fus}}$ (\hbar), $\langle l \rangle_{\text{fis}}$ (\hbar); prefission neutron multiplicity ν_{pre} ; loss in excitation energy due to evaporation of neutron, ΔE_{eva} ; l dependent fission barrier height $B_{f, \langle l_{\text{fis}} \rangle}$; and rotational energy of the compound nucleus, E_{rot} . Column 9 is the effective excitation energy of the fissioning nucleus relative to the height of the fission barrier, $E_{\text{sad}} = E_{CN}^* - B_{f, \langle l_{\text{fis}} \rangle} - \Delta E_{\text{eva}} - E_{\text{rot}}$; and the last column is the temperature of the compound nucleus at saddle given by $T = \sqrt{E_{\text{sad}}/a}$, where a is the level density parameter taken as $A_{CN}/8.5$. All the energies and temperatures are in MeV.

E_{Lab}	E_{CN}^*	$\langle l \rangle_{\text{fus}}$	$\langle l \rangle_{\text{fis}}$	ν_{pre}	ΔE_{eva}	$B_{f, \langle l_{\text{fis}} \rangle}$	E_{rot}	E_{sad}	T_{fis}
58	38.7	11.4	16.1	0.18	1.9	18.6	1.5	16.7	0.87
65	45.2	15.2	21.9	0.38	3.9	17.8	2.8	20.8	0.97
70	49.9	18.9	26.0	0.53	5.7	17.1	3.8	23.3	1.03
75	54.6	21.5	29.4	0.77	8.6	16.5	4.7	24.8	1.06

parameter q using the relation $q = (A^2\lambda)^{-1}$ is equal to 0.0092 ± 0.0003 , which is in good agreement with the value reported by Itkis *et al.* [10]. Thus the behavior of the widths also suggests the dominance of the LD mode.

D. Theoretical predictions for ^{187}Ir

Several theoretical predictions are available for fission of ^{187}Ir at low excitation energies. The peak positions of the different contributions, the underlying neutron-proton shells, are not expected to change with excitation energy. Further, the relative intensities are also not expected to be drastically different with the difference in a few MeV of excitation energy. Thus, the experimental and theoretical results at similar excitation energies can be compared qualitatively. The predictions of different theoretical models are shown in Fig. 5. The improved scission point model predicts asymmetric contribution peaking at $A_{L(H)} = 85$ (102) u [47], where $A_{L(H)}$ is the mass of the light (heavy) fragment. A calculation based on random walks over a five-dimensional (5D) macroscopic-microscopic potential-energy surface [27], has yielded asymmetric peak

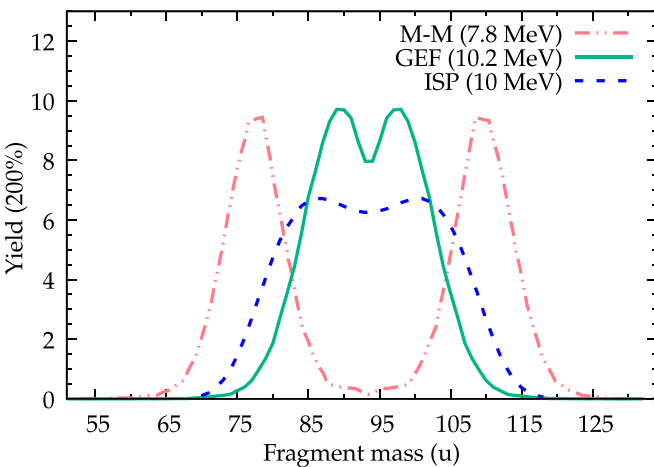


FIG. 5. Comparison of the available theoretical predictions for fission fragment mass distribution of ^{187}Ir . The predictions of the macroscopic-microscopic model (M-M) [27], GEF (Version 2021/1.1) [46], and improved scission point model (ISP) [47] are shown in dot-dot-dashed, solid, and dashed lines, respectively. The numbers in the brackets represent the excitation energy above the saddle point.

at mass $A_{L(H)} = 78$ (110) u. The authors of [27] attribute the origin of asymmetric fission in this region to the mass asymmetric saddle point. The general fission model (GEF) [46], which is based on a semiempirical approach, has also been employed to explain the observed mass distributions in the preactinide region [29]. As can be seen from Fig. 5, the distributions predicted by different models differs significantly. However, all the theoretical models predict a substantial microscopic contribution, which is not in agreement with the experimental observations. Further theoretical investigations are required to understand the experimental mass distributions for the light preactinides.

IV. SUMMARY AND CONCLUSION

To study the shell effects in the newly discovered asymmetric island which belongs to the sub-Pb region, we performed an experiment to populate the ^{187}Ir nucleus. The fission fragment mass and TKE distributions were used as a probe and the measurements were done at four laboratory energies 58, 65, 70, and 75 MeV. The experimental mass distributions were extracted using the time-difference method. Single Gaussian fits provide reasonably good description of the experiment mass and TKE distributions. The widths of the measured TKE distributions agree well with the systematic LD behavior. The observed widths of the mass distributions can also be explained using a statistical relation. These observations suggest the dominance of LD fission mode in the present case. Small contributions due to microscopic corrections from $Z = 38$ and 45 could be extracted when the widths of the LD component were fixed from the systematic behavior. However, the theoretical models predict substantial contributions from microscopic corrections. More studies are required to understand the evolution of the different contributions to the mass distribution across the preactinide region, especially in case of lighter preactinides.

ACKNOWLEDGMENTS

We thank P. Patale for his help during the experiment. The authors are thankful to the staff of BARC-TIFR Pelletron-LINAC facility, Mumbai, India for unwavering support during the experiment. We also thank the target laboratory, TIFR, Mumbai for target preparation. The authors S.D. and T.S. are

sincerely grateful to DST, Govt. of India for financial support under the DST-INSPIRE Fellowship scheme. Funding from

CSIR-UGC, India and UGC-DAE-CSR is acknowledged by authors S.K. and A.C. respectively.

- [1] L. Meitner and O. R. Frisch, *Nature (London)* **143**, 239 (1939).
- [2] N. Bohr and J. A. Wheeler, *Phys. Rev.* **56**, 426 (1939).
- [3] V. M. Strutinsky, *Nucl. Phys. A* **95**, 420 (1967).
- [4] U. Brosa, S. Grossmann, and A. Müller, *Phys. Rep.* **197**, 167 (1990).
- [5] K.-H. Schmidt and B. Jurado, *Rep. Prog. Phys.* **81**, 106301 (2018).
- [6] A. N. Andreyev, K. Nishio, and K.-H. Schmidt, *Rep. Prog. Phys.* **81**, 016301 (2018).
- [7] S. Kailas and K. Mahata, *Pramana* **83**, 851 (2014).
- [8] M. G. Itkis, V. N. Okolovich, and A. Y. Rusanov, *Z. Phys. A* **320**, 433 (1985).
- [9] M. G. Itkis, N. A. Kondratev, and S. I. Mulgin, *Yad. Fiz.* **52**, 944 (1990).
- [10] M. G. Itkis, N. A. Kondratev, S. I. Mulgin, V. N. Okolovich, A. Y. Rusanov, and S. G. N., *Yad. Fiz.* **53**, 1225 (1991).
- [11] S. I. Mulgin, K.-H. Schmidt, A. Grewe, and S. Zhdanov, *Nucl. Phys. A* **640**, 375 (1998).
- [12] A. N. Andreyev, J. Elseviers, M. Huyse, P. Van Duppen, S. Antalic, A. Barzakh, N. Bree, T. E. Cocolios, V. F. Comas, J. Diriken, D. Fedorov, V. Fedosseev, S. Franchoo, J. A. Heredia, O. Ivanov, U. Köster, B. A. Marsh, K. Nishio, R. D. Page, N. Patronis *et al.*, *Phys. Rev. Lett.* **105**, 252502 (2010).
- [13] K. Nishio, A. Andreyev, R. Chapman, X. Derkx, C. Düllmann, L. Ghys, F. Heßberger, K. Hirose, H. Ikezoe, J. Khuyagbaatar, B. Kindler, B. Lommel, H. Makii, I. Nishinaka, T. Ohtsuki, S. Pain, R. Sagaidak, I. Tsekhanovich, M. Venhart, Y. Wakabayashi *et al.*, *Phys. Lett. B* **748**, 89 (2015).
- [14] E. Prasad, D. J. Hinde, K. Ramachandran, E. Williams, M. Dasgupta, I. P. Carter, K. J. Cook, D. Y. Jeung, D. H. Luong, S. McNeil, C. S. Palshetkar, D. C. Rafferty, C. Simenel, A. Wakhle, J. Khuyagbaatar, C. E. Düllmann, B. Lommel, and B. Kindler, *Phys. Rev. C* **91**, 064605 (2015).
- [15] R. Tripathi, S. Sodaye, K. Sudarshan, B. K. Nayak, A. Jhingan, P. K. Pujari, K. Mahata, S. Santra, A. Saxena, E. T. Mirgule, and R. G. Thomas, *Phys. Rev. C* **92**, 024610 (2015).
- [16] I. Tsekhanovich, A. N. Andreyev, K. Nishio, D. Denis-Petit, K. Hirose, H. Makii, Z. Matheson, K. Morimoto, K. Morita, W. Nazarewicz, R. Orlandi, J. Sadhukhan, T. Tanaka, M. Vermeulen, and M. Warda, *Phys. Lett. B* **790**, 583 (2019).
- [17] S. Gupta, C. Schmitt, K. Mahata, A. Shrivastava, P. Sugathan, A. Jhingan, K. S. Golda, N. Saneesh, M. Kumar, G. Kaur, L. Stuttge, D. Arora, H. Arora, A. Chatterjee, K. Chauhan, S. K. Duggi, D. P. Kaur, V. Mishra, P. N. Patil, and K. Rani, *Phys. Rev. C* **100**, 064608 (2019).
- [18] S. Gupta, K. Mahata, A. Shrivastava, K. Ramachandran, S. K. Pandit, P. C. Rout, V. V. Parkar, R. Tripathi, A. Kumar, B. K. Nayak, E. T. Mirgule, A. Saxena, S. Kailas, A. Jhingan, A. K. Nasirov, G. A. Yuldasheva, P. N. Nadtochy, and C. Schmitt, *Phys. Lett. B* **803**, 135297 (2020).
- [19] B. M. A. Swinton-Bland, M. A. Stoyer, A. C. Berriman, D. J. Hinde, C. Simenel, J. Buete, T. Tanaka, K. Banerjee, L. T. Bezzina, I. P. Carter, K. J. Cook, M. Dasgupta, D. Y. Jeung, C. Sengupta, E. C. Simpson, and K. Vo-Phuoc, *Phys. Rev. C* **102**, 054611 (2020).
- [20] C. Schmitt, A. Lemasson, K.-H. Schmidt, A. Jhingan, S. Biswas, Y. H. Kim, D. Ramos, A. N. Andreyev, D. Curien, M. Ciemala, E. Clément, O. Dorvaux, B. De Canditiis, F. Didierjean, G. Duchêne, J. Dudouet, J. Frankland, B. Jacquot, C. Raison, D. Ralet, B.-M. Retailleau, L. Stuttgé, and I. Tsekhanovich, *Phys. Rev. Lett.* **126**, 132502 (2021).
- [21] T. N. Nag, R. Tripathi, S. Patra, A. Mhatre, S. Santra, P. C. Rout, A. Kundu, D. Chattopadhyay, A. Pal, and P. K. Pujari, *Phys. Rev. C* **103**, 034612 (2021).
- [22] A. A. Bogachev, E. M. Kozulin, G. N. Knyazheva, I. M. Itkis, M. G. Itkis, K. V. Novikov, D. Kumar, T. Banerjee, I. N. Diatlov, M. Cheralu, V. V. Kirakosyan, Y. S. Mukhamejanov, A. N. Pan, I. V. Pchelintsev, R. S. Tikhomirov, I. V. Vorobiev, M. Maiti, R. Prajapat, R. Kumar, G. Sarkar *et al.*, *Phys. Rev. C* **104**, 024623 (2021).
- [23] E. M. Kozulin, G. N. Knyazheva, I. M. Itkis, M. G. Itkis, Y. S. Mukhamejanov, A. A. Bogachev, K. V. Novikov, V. V. Kirakosyan, D. Kumar, T. Banerjee, M. Cheralu, M. Maiti, R. Prajapat, R. Kumar, G. Sarkar, W. H. Trzaska, A. N. Andreyev, I. M. Harca, A. Mitu, and E. Vardaci, *Phys. Rev. C* **105**, 014607 (2022).
- [24] P. Möller, J. Randrup, and A. J. Sierk, *Phys. Rev. C* **85**, 024306 (2012).
- [25] A. V. Andreev, G. G. Adamian, and N. V. Antonenko, *Phys. Rev. C* **86**, 044315 (2012).
- [26] G. Scamps and C. Simenel, *Phys. Rev. C* **100**, 041602(R) (2019).
- [27] P. Möller and J. Randrup, *Phys. Rev. C* **91**, 044316 (2015).
- [28] T. Ichikawa and P. Möller, *Phys. Lett. B* **789**, 679 (2019).
- [29] K. Mahata, C. Schmitt, S. Gupta, A. Shrivastava, G. Scamps, and K.-H. Schmidt, *Phys. Lett. B* **825**, 136859 (2022).
- [30] A. Jhingan, S. Kalkal, P. Sugathan, K. Golda, R. Ahuja, J. Gehlot, N. Madhavan, B. Behera, and S. Mandal, *Nucl. Instrum. Methods Phys. Res.: Sect. A* **745**, 106 (2014).
- [31] V. E. Viola, K. Kwiatkowski, and M. Walker, *Phys. Rev. C* **31**, 1550 (1985).
- [32] H. Kumar, S. A. Tali, M. A. Ansari, D. Singh, R. Ali, K. Kumar, N.P.M. Sathik, S. Parashari, A. Ali, R. Dubey, I. Bala, R. Kumar, R. P. Singh, and S. Muralithar, *Nucl. Phys. A* **960**, 53 (2017).
- [33] H. Kumar, S. A. Tali, M. Afzal Ansari, D. Singh, R. Ali, K. Kumar, N. P. M. Sathik, A. Ali, S. Parashari, R. Dubey, I. Bala, R. Kumar, R. P. Singh, and S. Muralithar, *Eur. Phys. J. A* **54**, 47 (2018).
- [34] R. K. Choudhury, A. Saxena, A. Chatterjee, D. V. Shetty, S. S. Kapoor, M. Cinausero, L. Corradi, E. Farnea, E. Fioretto, A. Gadea, D. Napoli, G. Prete, A. M. Stefanini, D. Bazzaco, S. Beghini, D. Fabris, G. Montagnoli, G. Nebbia, C. Rossi-Alvarez, F. Scarlassara *et al.*, *Phys. Rev. C* **60**, 054609 (1999).
- [35] J. F. Ziegler, M. Ziegler, and J. Biersack, *Nucl. Instrum. Methods Phys. Res.: Sect. B* **268**, 1818 (2010).
- [36] R. Vandenbosch and J. Huizenga, *Nuclear Fission* (Academic, New York, 1973)
- [37] R. du Rietz, E. Williams, D. J. Hinde, M. Dasgupta, M. Evers, C. J. Lin, D. H. Luong, C. Simenel, and A. Wakhle, *Phys. Rev. C* **88**, 054618 (2013).

- [38] J. Töke, R. Bock, G. X. Dai, A. Gobbi, S. Gralla, K. D. Hildenbrand, J. Kuzminski, W. F. J. Muller, A. Olmi, H. Stelzer, B. B. Back, and S. Bjornholm, *Nucl. Phys. A* **440**, 327 (1985).
- [39] M. G. Itkis and A. Y. Rusanov, *Phys. Part. Nucl.* **29**, 160 (1998).
- [40] K. Hagino, N. Rowley, and A. Kruppa, *Comput. Phys. Commun.* **123**, 143 (1999).
- [41] K. Mahata and S. Kailas, *Phys. Rev. C* **95**, 054616 (2017).
- [42] A. Gavron, *Phys. Rev. C* **21**, 230 (1980).
- [43] P. Möller, A. J. Sierk, T. Ichikawa, A. Iwamoto, and M. Mumpower, *Phys. Rev. C* **91**, 024310 (2015).
- [44] A. J. Sierk, *Phys. Rev. C* **33**, 2039 (1986).
- [45] G. N. Knyazheva, E. M. Kozulin, R. N. Sagaidak, A. Y. Chizhov, M. G. Itkis, N. A. Kondratiev, V. M. Voskressensky, A. M. Stefanini, B. R. Behera, L. Corradi, E. Fioretto, A. Gadea, A. Latina, S. Szilner, M. Trotta, S. Beghini, G. Montagnoli, F. Scarlassara, F. Haas, N. Rowley *et al.*, *Phys. Rev. C* **75**, 064602 (2007).
- [46] K.-H. Schmidt, B. Jurado, C. Amouroux, and C. Schmitt, *Nucl. Data Sheets* **131**, 107 (2016).
- [47] A. V. Andreev, G. G. Adamian, and N. V. Antonenko, *Phys. Rev. C* **93**, 034620 (2016).